

HURRI-GAN: A Novel Approach for Hurricane Bias-Correction Beyond Gauge Stations using Generative Adversarial Networks

Noujoud Nader^{a,*}, Hadi Majed^b, Stefanos Giaremis^{c,d}, Rola El Osta^b, Clint Dawson^f, Carola Kaiser^a and Hartmut Kaiser^{a,e}

^aCenter of Computation and Technology, Louisiana State University, Baton Rouge, 70803 LA, US

^bSaint-Joseph University of Beirut, Beirut, 1104, Lebanon

^cDepartment of Physics, Aristotle University of Thessaloniki, Thessaloniki, 54124, Greece

^dCenter for Interdisciplinary Research and Innovation, Aristotle University of Thessaloniki, Thessaloniki, 57001, Greece

^eDepartment of Computer Science, Louisiana State University, Baton Rouge, 70803 LA, US

^fOden Institute for Computational Engineering and Sciences, The University of Texas at Austin, Austin 78712, TX, USA

ARTICLE INFO

Keywords:

Time Generative Adversarial Networks

Extrapolation

Offset time series

ADCIRC forecasting

ABSTRACT

The coastal regions of the eastern and southern United States are impacted by severe storm events, leading to significant loss of life and properties. Accurately forecasting storm surge and wind impacts from hurricanes is essential for mitigating some of the impacts, e.g., timely preparation of evacuations and other countermeasures. Physical simulation models like the ADCIRC hydrodynamics model, which run on high-performance computing resources, are sophisticated tools that produce increasingly accurate forecasts as the resolution of the computational meshes improves. However, a major drawback of these models is the significant time required to generate results at very high resolutions, which may not meet the near real-time demands of emergency responders. The presented work introduces HURRI-GAN, a novel AI-driven approach that augments the results produced by physical simulation models using time series generative adversarial networks (TimeGAN) to compensate for systemic errors of the physical model, thus reducing the necessary mesh size and runtime without loss in forecasting accuracy. We present first results in extrapolating model bias corrections for the spatial regions beyond the positions of the water level gauge stations. The presented results show that our methodology can accurately generate bias corrections at target locations spatially beyond gauge stations locations. The model's performance, as indicated by low root mean squared error (RMSE) values, highlights its capability to generate accurate extrapolated data. Applying the corrections generated by HURRI-GAN on the ADCIRC modeled water levels resulted in improving the overall prediction on the majority of the testing gauge stations. Such a model can act in conjunction with a temporal prediction approach as a component for real-time full spatiotemporal bias corrections to a physics-based model for operational forecasting systems. Moreover, it can potentially reduce the required resolution of the applied computational meshes without losing accuracy while also providing useful insight regarding the behavior of biases for future developments in storm surge modeling. The source code is available on GitHub¹ or Zenodo², respectively.

1. Introduction

Tropical cyclones are extreme weather events that affect coastal communities around the globe. In the United States alone, the associated annual damages between 1980 and 2024 have been estimated to exceed \$31 billion with 154 deaths per year on average, with these numbers being almost doubled in the last 20 years [1]. Moreover, severe storms, tropical cyclones and flooding constitute the top three natural disasters in descending order of occurrence frequency among all the billion-dollar disaster events that have taken place in the United States from 1980 to 2023, with two of these event types leading the list in both the total number of human casualties and total financial losses per year [2]. Rise in sea surface temperature and other projected climate changes are predicted to increase the frequency of intense hurricanes

¹https://github.com/NoujoudNader/Extrapolation_GAN

²<https://doi.org/10.5281/zenodo.15634528>

✉ nnader@lsu.edu (N. Nader); hadi.majed@net.usj.edu.lb (H. Majed); sgiaremi@physics.auth.gr (S. Giaremis); rola.osta@usj.edu.lb (R.E. Osta); clint@oden.utexas.edu (C. Dawson); ckaiser@cct.lsu.edu (C. Kaiser); hkaiser@cct.lsu.edu (H. Kaiser)

ORCID(s): 0009-0000-4687-1416 (N. Nader); 0000-0002-0107-3127 (S. Giaremis); 0000-0001-7273-0684 (C. Dawson); 0000-0002-8712-2806 (H. Kaiser)

and the magnitude of storm surge [3, 4]. Therefore, the need for continuous improvement of numerical storm surge prediction frameworks in the context of operational warning systems is ongoing [5].

Storm surge numerical models are typically based on the shallow-water equations in barotropic, depth-integrated form, with forcing from wind and atmospheric pressure, bottom drag, tides, and wind waves [6, 7]. The ADvanced CIRCulation model for oceanic, coastal and estuarine waters (ADCIRC) is a high-fidelity hydrodynamic model that solves the shallow-water equations within the continuous Galerkin, linear finite element method on unstructured meshes, [8]. This approach has been extensively used for storm surge modeling [9–11]. ADCIRC is the main physics-based workhorse in many real-time forecasting frameworks, such as Coastal Emergency Risk Assessment (CERA). CERA is an interactive web visualization platform combining measurements from sources such as water level gauge stations and tide, wind-wave and hurricane storm surge numerical predictions, designed to provide first responders, decision makers and the general public with critical insights during hurricanes and extreme weather events [12]. The CERA framework has also been recently used for the development of a historical storm archive containing hindcasts of more than 60 storms over the last 20 years [13, 14].

Recent improvements in storm surge and ocean circulation modeling in terms of mesh design and treatment of the description of natural processes have significantly improved accuracy and computational efficiency [15–18]. However, inherent uncertainties, although minimized, are inevitably present and well documented [19]. These can be due to inaccuracies in the description of hurricane characteristics such as track and wind speed and/or inputs such as description of coastal elements and land cover specification [20–23]. Another source of uncertainty can be due to unresolved drivers such as rainfall, large-scale oceanic motions, and hydrological input, which are often not explicitly treated in storm surge models to restrict the complexity and computational cost of the model [24]. Neglecting uncertainties has been shown to lead to biases that have a substantial impact on storm surge predictions and risk assessment [25]. Therefore, detecting and quantifying these uncertainties is essential for improving the reliability of storm surge forecasting.

Traditional approaches for treating uncertainties and biases involve ensemble forecasting, data assimilation and other statistical methods such as quantile mapping [23, 24, 26–28]. More recently, machine learning (ML) approaches have been also explored for this purpose, showing improved accuracy in comparison with previous state-of-the-art statistical methods [29]. Commonly used ML architectures involve deep convolutional neural networks (CNNs), long-short term memory (LSTM) networks, bagged regression trees and multilayer perceptrons (MLPs) [29–33]. Generative adversarial networks (GANs) constitute an emerging and highly promising type of neural networks for inferring the probability distribution that a given training set is drawn from, based on game theory – in addition to traditional optimization techniques [34, 35]. Despite originally implemented mostly for 2D/3D image reconstruction applications, GAN-based models have been recently shown promising performance for spatially bias correcting temperature, precipitation and wind predictions from climate models based on observed data [36–39].

Motivation. Previously, our group has demonstrated the viability of using LSTM-based models for predicting the offsets between observed and simulated water level values in gauge stations based on their past values, trained on historical storm data from the CERA platform [30]. In this work, we propose a novel approach, HURRI-GAN, based on TimeGAN [40], an extension of the original GAN approach for treating time-sequence data, to learn the correspondence between the aforementioned offset time series and geographic coordinates, so it can generate the temporal behavior of the former at arbitrarily given coordinates. In this way, offset time series at gauge stations could be extrapolated to any desired mesh point. To our knowledge, this is the first report of applying the TimeGAN approach for bias correcting water level data via spatiotemporal extrapolation. These results aim towards the development of improved bias correction components in real-time forecasting frameworks.

We summarize the main contributions of this paper as follows:

- We propose a novel approach for bias correction based on generative artificial intelligence (GenAI), called HURRI-GAN, designed for spatiotemporal extrapolation of water level offsets.
- We introduce a new application of TimeGAN for hurricane-induced storm surge bias correction, where the model learns the mapping between sequential offset time series and geographic coordinates – enabling offset generation at unseen locations on the mesh.
- We leverage historical storm data from the CERA platform for both model training and validation.

- We demonstrate the feasibility of AI-enhanced storm surge bias correction within real-time forecasting frameworks, especially for coastal regions beyond gauge stations aiming to improve the accuracy, reliability, and spatial coverage of storm surge predictions.

2. Data and Methodology

2.1. Overview

Figure 1 illustrates the methodology framework for HURRI-GAN proposed in this paper. It comprises three key steps, namely data pre-processing, modeling, and extrapolation. The first stage (Figure 1.A) involves the systematic extraction of the offsets (Eq. 2.1) between the modeled and observed water elevation time series from each gauge station in the available dataset. The offset time series for each gauge station is defined as follows:

$$H_{\text{offset}}(t) = H_{\text{modeled}}(t) - H_{\text{observed}}(t) \quad (2.1)$$

where $H_{\text{modeled}}(t)$ and $H_{\text{observed}}(t)$ are the forecast (via ADCIRC) and observed (from gauge stations) water levels, respectively, and $H_{\text{offset}}(t)$ is the water level offset (i.e., the bias), at each timestep, t . More details on this phase are explained in Section 2.2. In this work, we demonstrate the application of our newly proposed HURRI-GAN model to extrapolate previous ML-predicted biases to arbitrary spatial coordinates. We use our previous LSTM-based model [30] to forecast the complete offset signals at the gauge stations, which, in turn are used to train our newly proposed GenAI model after appropriate reshaping and preprocessing (Section 2.2.2). The GenAI model built to address our extrapolation problem is based on the TimeGAN approach [40] and constitutes the HURRI-GAN model. The processed samples are passed to the HURRI-GAN model for training and testing to assess its extrapolation performance. The gauge stations are divided into training and testing subsets. Testing is performed on the the testing gauge stations, which are not included by any means in the training of the model (see Section 2.2.1), so that corrected water level forecasts can be directly evaluated against their observed counterparts. The structure and parameters of the model are optimized during this phase (Figure 1.B). For more details, we refer to Section 2.3. Once trained, the model can be applied for spatial extrapolation by giving as input only the coordinates of an arbitrary mesh point. After generating the offsets $H_{\text{generated offsets}}(t)$, the corrected forecast water level data, $H_{\text{corrected}}(t)$, are calculated according to the following equation:

$$H_{\text{corrected}}(t) = H_{\text{modeled}}(t) - H_{\text{generated offset}}(t) \quad (2.2)$$

. The model's extrapolation performance is evaluated based on the corrected water levels (Eq. 2.2) for the selected testing gauge stations (Figure 1.C).

2.2. Data

For this analysis, we use water level data for six hurricanes, obtained from the Historical Storm Surge Archive by [13] and visualized through the built-in interface with the CERA website [12]. The hurricane data includes both modeled and observed water level values. The modeled values are produced by ADCIRC [8]. Observed data are obtained from different agencies including the National Oceanic and Atmospheric Administration (NOAA) [41], coastal gauge stations (USGS) [42], U.S. Army Corps of Engineers (USACE) [43], Texas Coastal Ocean Observation Network (TCOON) [44], and Puerto Rico Seismic Network (PRSN) [45]. Both data sets are collected at hourly intervals. Offsets, as defined by Eq. 2.1, are calculated by taking the difference between observed and modeled water level at each hourly time interval. This process resulted in the creation of an offset time series for each gauge station available during each hurricane. Gauge stations with missing offset values are excluded from the analysis. Additionally, an extra filtering step is performed to eliminate the influence of gauge stations that exhibited abnormal offset values. Stations with identified offset outlier values are also removed from this analysis. Table 1 presents the hurricanes used in this study, along with the corresponding number of stations and the total amount of hourly offsets data collected for each hurricane after preprocessing.

2.2.1. Clustering

The next step is to split the gauge stations within each hurricane into training and testing sets. As we are working with a GenAI model, we need to provide more training data than usual, as the task requires more data for proper

Table 1

Hurricanes considered in this study, their category based on the Saffir-Simpson hurricane scale [46], the number of station and the total amount of hourly offset data in each.

Hurricane	Category	No. of stations	No. of hourly offsets
Ian (2022)	H5	250	26250
Harvey (2017)	H4	247	25935
Ida (2021)	H4	264	18216
Idalia (2023)	H4	304	31920
Matthew (2016)	H4	236	24780
Hermine (2016)	H1	259	27195

learning. For this, a split of 90% of the stations set for training and 10% for testing is mainly chosen. To ensure that each region in the studied geographic area is properly represented, we employ the K-means clustering algorithm [47] to geographically divide the stations into groups. The gauge stations are clustered into groups based on their coordinates, with the condition that each cluster contains more than one station. For each hurricane, the number of clusters is 10% of the number of stations. This clustering approach helps to ensure that the testing stations are not concentrated in a single region but are representative of the entire geographic study area. From each cluster, one station is randomly selected and designated as a testing station while the remaining stations are added to the training set. An example of the clustering process for Hurricane Harvey(2017) is illustrated in Figure 2, where the stations are divided into 24 clusters based on their coordinates, ensuring a proper representation of all geographical areas in the testing set. Each cluster group is presented with a different color.

2.2.2. Preprocessing

After splitting the gauge stations into training and testing sets, the offsets are normalized for each hurricane. MinMax scaling from Scikit-Learn [48] is used on the training and testing data separately to avoid data leakage. The time series data for each gauge station is then reshaped into a 2D array format to be compatible with the input requirements of the model [40]. In this case, data from each gauge station are fed into the model as a unique input, with its offset data reshaped into a (5×21) array for most hurricanes, where the total signal length is 105. For Hurricane Idalia, which has a signal length of 69 hours, the data is reshaped into a (3×23) array. The data is then distributed into batches, with the batch size set to 10. The choice of batch size ensures efficient model training while managing memory consumption. As for the coordinates, four static embeddings were retrieved from each pair and are repeated for each row in the input matrix. For each timestep in this matrix, the model can properly relate the coordinate's embeddings to the temporal sequence. Having a large number of embeddings will make it too complicated for the model to learn, while having different embeddings for each timestep will result in the model failing to capture consistent spatial understanding. Finally, each batch contains the gauge station's coordinate tuple (x, y) paired with its corresponding offset matrix. The input shape for each sample is as follows:

$$\begin{bmatrix} o_{1,1} & \cdots & o_{1,21} \\ o_{2,1} & \cdots & o_{2,21} \\ \vdots & \ddots & \vdots \\ o_{5,1} & \cdots & o_{5,21} \end{bmatrix} \begin{bmatrix} y_1 & \cdots & y_4 \\ y_1 & \cdots & y_4 \\ \vdots & \ddots & \vdots \\ y_1 & \cdots & y_4 \end{bmatrix}$$

2.3. GenAI models

Generative artificial intelligence (GenAI) models represent a groundbreaking stride in the realm of artificial intelligence, facilitating the creation of novel data rather than solely interpreting existing information. Notable examples such as GANs and sophisticated autoregressive models like the distinguished OpenAI GPT series excel in generating lifelike images, text, music, and diverse content forms. By discerning intricate patterns from extensive datasets, these generative AI models exhibit the capacity to craft outputs that often mirror human-created content. This innovation carries profound implications spanning various domains, including art, design, content generation, and its potential utility in accelerating drug discovery and scientific exploration [49, 50]. In the following, we will discuss the overview of TimeGAN components, and the proposed HURRI-GAN structure.

2.3.1. Overview of TimeGAN Components

To address the challenge of generating data that matches the temporal distribution of a real data sample, Yoon and Jarrett [40] proposed a new GAN architecture called TimeGAN. In traditional GANs [34], a neural network, referred to as the generator (G), aims to map random noise to a target distribution. An auxiliary neural network, known as the discriminator (D), guides the training of G by distinguishing between the generated data and the real data (i.e. offsets). This process, known as adversarial learning, involves G being trained not toward a fixed objective, but rather to fool D, which is concurrently updated to improve its discrimination capabilities.

TimeGAN [40] introduces three additional components with corresponding loss functions. The embedder (E) and recovery (R) models together form what is known as an autoencoder. The embedder's role is to map real data samples, which incorporate both temporal and static features, into an abstract representation known as the latent space. This space contains latent codes or embeddings. Specifically, the embedder maps both temporal features (time series offsets) and static features (gauge station coordinates) into this latent space, while the recovery model reconstructs these embeddings back into their original representations. As the feedback from the discriminator D may not be enough, a new component, the supervisor (S), is introduced to bridge the gap between the autoencoder and adversarial networks. This supervisor helps the embedder generate better embeddings, which in turn improves the learning process for the generator.

2.3.2. Proposed HURRI-GAN structure

A detailed structure of the network for each temporal component used in HURRI-GAN is presented in Table 2. The embedder component, as the generator and recovery, consists of two neural networks, one that deals with the temporal data (i.e. offsets time-series) and one with the static data (i.e. the stations coordinates). The static network is a simple dense layer with four neurons and 'sigmoid' activation function that maps the coordinate components into four latent representations or two reconstructed coordinates for the recovery. The temporal network is a much more complex model with multiple Gated Recurrent Unit (GRUs) layers followed by a dense layer with a number of neurons equal to the number of columns in the input matrix (Section 2.2). The supervisor follows the same architecture but with a smaller number of GRU layers. The discriminator architecture consists of only a temporal network with a two bi-directional GRU layers, followed by a dense layer with one neuron corresponding to its binary classification task. For all of the components containing static networks, the coordinate input passes first through the static network. The resulting output is concatenated with the temporal input, and fed into the temporal networks that will study the relationship between the two types of inputs and provide the results accordingly. The structure and the number of neurons were selected based on hyperparameter tuning (Section 3.2).

To train the HURRI-GAN model, we first train the autoencoder (E and R). The autoencoder learns from real data (offsets) by minimizing temporal and static embedding losses, both calculated using mean squared error (MSE, Eq. 2.4). The autoencoder's parameters are updated based on the gradients to minimize the loss. Alternatively, we train S using real embeddings from the embedder by minimizing the MSE loss (Eq. 2.4). Finally, all the components are trained together. The generator and embedder are trained more frequently than the discriminator, which is only trained when its loss exceeds a threshold. The generator's loss is computed from a combination of adversarial, supervisor, and distribution losses, while the discriminator's loss is based on comparing values of Binary Cross-Entropy (BCE):

$$\text{BCE} = -\frac{1}{n} \sum_{i=1}^n [y_i \log(\hat{y}_i) + (1 - y_i) \log(1 - \hat{y}_i)] \quad (2.3)$$

across real and generated data. In Eq. 2.3, y represents the real label of the data and \hat{y} represents the predicted label of the data. The Adam optimizer [51] was used for all of the compiled models during training.

2.4. Evaluation Parameters and Computational Details

Mean square Error (MSE, Eq. 2.4), root mean squared error (RMSE, Eq. 2.5) and mean absolute errors (MAE, Eq. 2.6) are used here as metrics to evaluate the model performance. Smaller values of errors mean higher generation accuracy.

$$\text{MSE} = \frac{1}{n} \sum_{i=1}^n (y_i - \hat{y}_i)^2 \quad (2.4)$$

Table 2

Schematic overview of the structure of the HURRI-GAN model (GRU: Gate Recurring Unit, Bi-GRU: Bidirectional Gated Recurrent Unit).

Embedder, Recovery, Generator			
Layers	No. of Neurons	Activation	Output Shape
GRU	256	–	5*256
GRU	256	–	5*256
GRU	256	–	5*256
GRU	256	–	5*256
GRU	256	–	5*256
Dense	21	Sigmoid	5*21

Supervisor			
Layers	No. of Neurons	Activation	Output Shape
GRU	256	–	5*256
GRU	256	–	5*256
GRU	256	–	5*256
GRU	256	–	5*256
Dense	21	Sigmoid	5*21

Discriminator			
Layers	No. of Neurons	Activation	Output Shape
Bi-GRU	256	–	5*512
Bi-GRU	256	–	1*512
Dense	1	Sigmoid	1*1

$$RMSE = \sqrt{\frac{1}{n} \sum_{i=1}^n (y_i - \hat{y}_i)^2}. \tag{2.5}$$

$$MAE = \frac{1}{n} \sum_{i=1}^n |y_i - \hat{y}_i| \tag{2.6}$$

To evaluate the general performance of the extrapolation model HURRI-GAN, we first evaluated MSE and MAE between real and generated offsets. In this case, y represents the real offset values, \hat{y} stands for the extrapolated (predicted) offset values and n denotes the total number of samples. Then we evaluated the bias correction after generation, these evaluation metrics are estimated between the corrected forecast (Eq. 2.2) and the original forecast (produced by ADCIRC) . Herein, y represents the original forecast values (without AI), \hat{y} stands for the the corrected forecast (with AI).

The HURRI-GAN model is implemented using TensorFlow 2.16.2 with Keras in Python 3.9.18.

3. Results and Discussion

3.1. LSTM-based model results

As a first step, offsets predictions at known gauge station locations are generated by using our previously developed LSTM-based model [30]. To estimate the accuracy of the LSTM-based model, the evaluation metrics between real and LSTM-generated offsets for each hurricane, including MSE, RMSE, and MAE, are presented in Table 3. As shown in Table 3, the LSTM-based model demonstrated strong performance across all storms, yielding consistently low MSE, RMSE, and MAE values. These results, which are in agreement with our previously published results, confirm the LSTM-based model’s reliability and suitability for generating offset time series to train HURRI-GAN.

Table 3

Metrics in feet of the real vs ML-predicted offsets generated via our previous LSTM-based model [30] for each of the considered hurricanes.

Hurricane	MSE	RMSE	MAE
Ian (2022)	0.129	0.359	0.241
Harvey (2017)	0.121	0.347	0.214
Ida (2021)	0.116	0.34	0.197
Idalia (2023)	0.124	0.352	0.22
Matthew (2016)	0.066	0.257	0.169
Hermine (2016)	0.085	0.292	0.177

3.2. Hyperparameter tuning

To optimize our network architecture for each component in HURRI-GAN, we conduct hyperparameters tuning for each hurricane. In this process, stations are divided into training and testing sets. Subsequently, candidate models with different hyperparameters are trained on the former and tested on extrapolating data on the latter. Tuning is performed separately for each of the hurricane considered in this work. The parameters tuned during this process include the number of layers, number of neurons and number of epochs. The number of layers is analysed for the generator, embedder and recovery. The supervisor is one layer less than the other components. The discriminator is two layers. The architecture that gives the lowest RMSE in most cases is finally selected.

In our analysis (Table 4), it is observed that using 2000 training epochs for the joint training phase does not lead to the best performance for most hurricanes, suggesting that more training epochs are needed to adequately capture the complexity of the storm surge data. Moreover, the results from the hyperparameter tuning process reveal that the optimal architecture varies in terms of layers, neurons, and epochs, highlighting the importance of conducting hurricane-specific hyperparameter optimization to ensure the best possible extrapolation performance within each hurricane. More specifically, for some hurricanes, a model with four layers provides the best performance (Hurricane Harvey (2017), Idalia (2023), Matthew (2016), and Hermine (2016)), while others require five layers to effectively capture the underlying data distribution (Table 4). Similarly, the optimal number of neurons and epochs varies depending on the complexity of the hurricane's data. However, the choice of 256 neurons and 3000 epochs is generally shown to yield optimal results for most storms (Table 4). Therefore, using the aforementioned settings, along with using 4 or 5 layers, would be expected to yield optimal results for a new storm in a real-world scenario.

3.3. Extrapolation analysis

In this section, the behavior of the best model variation for each hurricane, based on the discussion in the previous section, will be analyzed in further detail. From Table 4, it can be seen that, overall, the HURRI-GAN architecture demonstrates promising performance across all hurricanes, with the lowest RMSE (0.275 ft. or 0.083 m.) observed for Hurricane Matthew (2016), where the model effectively captures the storm surge dynamics with minimal error, thus indicating strong predictive accuracy for extrapolation. On the other hand, the model exhibits the highest RMSE (0.654 ft. or 0.199 m.) for Hurricane Ian (2022).

To evaluate the performance of the model at individual locations, we analyze the RMSE of the extrapolated offsets generated by HURRI-GAN for each testing gauge station. Figure 3 presents the geographical distribution of the RMSE of the extrapolated offsets in each station for each hurricane, along with the corresponding station agency and the hurricane track [14, 41].

Typically, RMSE values below 1.5 ft. (0.46 m) are observed in most cases. However, in some cases, stations located along the hurricane's path tend to have relatively higher RMSE values compared to those situated further inland or outside the path. This is expected due to the increased complexity of storm surge dynamics in areas affected directly by the hurricane, particularly near landfall. For example, in the case of Hurricane Ida (2021), stations near the path of the hurricane (especially New Orleans at Louisiana) exhibit higher RMSE values. Moreover, a few outliers are observed, such as for Hurricanes Harvey (2017) and Ida (2021), in South Carolina and Georgia, respectively. Stations with higher RMSE values, not located directly in the path of the hurricane, are also observed in some other cases (such as for Hurricane Ian (2022) in a few stations in Texas, Louisiana and Virginia), although with not so pronounced RMSE

Table 4

Hyperparameter tuning results for the HURRI-GAN model. The table presents the RMSE values (in feet) along with the optimal hyperparameters for each hurricane, including the number of network layers, number of neurons, and number of epochs. The values for each of the aforementioned parameters considered in this analysis are listed in brackets. The number of layers is analyzed for Generator, Embedder and Recovery. The supervisor is one layer less than the other components, while the discriminator architecture always consists of two layers.

	Error Metric	RMSE (ft.)	Parameters		
			No. of Layers [4, 5]	No. of neurons [128, 256]	No. of Epochs [2000, 3000, 4000]
Ian(2022)	Min	0.654	5	256	4000
	Max	0.724	4	128	4000
	Mean - Std	0.669	5	256	3000
	Mean + Std	0.707	4	256	2000
Harvey(2017)	Min	0.356	4	256	3000
	Max	0.459	5	128	2000
	Mean - Std	0.36	5	256	3000
	Mean + Std	0.415	4	128	3000
Ida(2021)	Min	0.623	5	128	3000
	Max	0.809	4	128	3000
	Mean - Std	0.65	4	256	3000
	Mean + Std	0.749	5	128	4000
Idalia(2023)	Min	0.362	4	256	4000
	Max	0.523	5	128	2000
	Mean - Std	0.362	4	256	4000
	Mean + Std	0.431	5	128	4000
Matthew(2016)	Min	0.275	4	128	3000
	Max	0.465	5	128	3000
	Mean - Std	0.291	4	256	2000
	Mean + Std	0.417	4	256	3000
Hermine(2016)	Min	0.368	4	128	3000
	Max	0.477	5	256	2000
	Mean - Std	0.374	4	256	4000
	Mean + Std	0.447	4	256	2000

values. Typically these cases correspond to stations located further inland or in areas with complex coastline features involving elements such as levies and jetties.

To further investigate this behavior, Figure 4 provides a more detailed view of the distribution of RMSE across different hurricanes and agencies. Each boxplot represents the RMSE distribution of testing stations for a given hurricane. The spread of values within each plot illustrates the variability in forecast accuracy across different locations. In the case of Hurricane Harvey (2017), higher RMSE values are typically found at stations located along the storm track, reflecting the greater complexity of storm surge dynamics near landfall. However, a common and consistent trend across all the considered hurricanes is that the highest RMSE values are predominantly observed at USGS stations, regardless whether the stations are in proximity to the storm track or not. USGS stations are often located further inland, e.g., along rivers, or in coastal areas with intricate coastline features, and thus governed by different hydrodynamical laws compared to stations more directly exposed to the ocean.

To evaluate how hurricane intensity impacts the extrapolating capabilities of HURRI-GAN, in Figure 5, we demonstrate the effectiveness of the ML extrapolated water level corrections for two stations per each of three of the considered hurricanes, Hermine (2016), Harvey (2017) and Ian (2022), which lie towards the two ends of the Saffir-Simpson scale (H1, H4 and H5, respectively) [46]. Both stations for each hurricane are selected so to be in close geographical proximity to the corresponding storm track and simultaneously focusing on both heavily affected areas and less severely impacted regions. By comparing the evaluation metrics of the non-bias corrected water level water level forecasts with the bias corrected ones with HURRI-GAN, it is evident that the HURRI-GAN extrapolation model is capable of improving predictions by reducing RMSE by $\sim 0.2 - 1.1$ ft. (0.06 – 0.33 m) (Figure 5). This behavior is consistent regardless of storm intensity, although generated bias corrections are slightly less pronounced for the highest intensity hurricane (Hurricane Ian, 2022, H5). Moreover, the model can produce adequate corrections for both areas with high storm surge (e.g., USCG station Hatteras (NOAA) during Hurricane Hermine (2016) Figure 5a) and less severely affected locations (e.g., Clearwater Beach (NOAA) during Hurricane Ian (2022), Figure 5c).

3.4. Inference Performance Analysis for Extrapolation with HURRI-GAN

In real-world applications, the ability to quickly extrapolate storm surge predictions for a large number of locations is critical. Therefore, an important aspect of evaluating HURRI-GAN is analyzing the time required for inference, which directly impacts the feasibility of using the model in the context of operational forecasting systems. In Figure 6, we present the computational time required for the HURRI-GAN model to generate inferences as a function of the amount of coordinates. As expected, inference time increases with the number of coordinates at an exponential-like rate. Despite that a noticeable increase in inference time is observed when the model is required to generate more than 10^4 values, the total inference time for 10^5 values remains at a reasonable time of 5160 seconds (i.e., 1 h 40 min) and can potentially be further reduced by implementing additional parallelization schemes. This amount of data points could produce a high density coverage of a computational mesh spanning a wide enough region of interest during a storm. Moreover, given that forecasts from physics-based models (e.g., ADCIRC) are typically produced every 6 hours or so and station-wise offset prediction models such as our previous LSTM-based approach [30] have an almost negligible inference time, the inference time required for extrapolating offsets with HURRI-GAN is reasonable to allow its use as an additional bias correction component in an operational forecasting framework.

4. Conclusion

In this work, we explore the use of Generative AI (GenAI) methods through HURRI-GAN (Hurricane Bias Correction Beyond Gauge Stations Using Generative Adversarial Networks) to address the challenge of extrapolating bias-corrected water-level predictions to arbitrary geographic coordinates in storm surge modeling. HURRI-GAN is intended to be used in conjunction with a post-processing, station-wise bias estimator, such as our previously proposed LSTM-based model [30], for estimating bias beyond gauge station locations. With HURRI-GAN, we introduce the use of a generative model based on the TimeGAN approach [40] to extrapolate the behavior of the systemic error in storm tide forecast models, thereby enhancing the forecasting accuracy in areas without reference gauge stations during hurricane events.

The dataset from the Historical Storm Surge Archive [13] is used for the training and evaluating the proposed TimeGAN model. This dataset includes storm tide forecasts generated by ADCIRC [9], and observed water level data obtained from gauge stations. Here we consider data from Hurricanes Matthew (2016), Hermine (2016), Harvey (2017), Ida (2021), Ian (2022) and Idalia (2023). The offset time series for all hurricanes are initially extracted using Eq. 2.1. Subsequently, we employ our previously developed LSTM-based model ([30]) to generate offset prediction signals for each station and each of the considered hurricane. The stations are then clustered into groups, with one station per group designated for the test set and the remaining stations included in the training set. Subsequently, the data undergo normalization, cleaning, and reshaping to prepare it for input into HURRI-GAN. The TimeGAN-based structure and model parameters are finally chosen after hypertuning for each hurricane. We demonstrate that using an architecture with 256 neurons, 3000 epochs and 4 or 5 layers leads to the most accurate predictions in most cases, so it would be recommended for a real-world scenario. Our results show that our methodology can accurately extrapolate previously station-wise generated offsets at testing gauge station locations, unknown to the model during training, with satisfactory accuracy. Applying extrapolated bias corrections can consistently lead to a reduction of forecast RMSE, with little influence of the hurricane intensity. Inference times remain reasonable even for a large number of inferences (1h and 40 mins for 10^5 inferences).

Limitations and future work: Limited performance is observed in few cases for stations along hurricane tracks or in locations further inland from the coastline or impacted by subtle coastline features. Therefore future work could focus on enhancing the robustness of the model by incorporating more diverse datasets, including data from different types of storms and geographical regions. Moreover, additional optimization could further improve inference times. Finally, implementing HURRI-GAN into real-time forecasting and evaluating its performance in operational settings would also be valuable directions for future research.

5. Acknowledgments

We acknowledge the support of the Department of Energy (DoE) through the award DE-SC0022320 (MuSiKAL). We would also like to thank Louisiana State University (LSU) and the Center for Computation and Technology at LSU for granting allocations for their computing resources and storage space.

CRedit authorship contribution statement

Noujoud Nader: Methodology, Software, Validation, Formal analysis, Investigation, Visualization, Writing - Original Draft. **Hadi Majed:** Methodology, Software, Validation, Formal analysis, Investigation, Visualization. **Stefanos Giaremis:** Methodology, Formal analysis, Investigation, Writing - Original Draft. **Rola El Osta:** Formal analysis, Investigation. **Clint Dawson:** Project administration, Funding acquisition. **Carola Kaiser:** Visualization, Supervision, Data Curation. **Hartmut Kaiser:** Conceptualization, Supervision.

References

- [1] NOAA National Centers for Environmental Information (NCEI). U.S. billion-dollar weather and climate disasters, 2024. URL <https://www.ncei.noaa.gov/access/billions/summary-stats/US/2004-2024>.
- [2] Adam B. Smith. U.S. billion-dollar weather and climate disasters, 1980 - present (ncei accession 0209268), 2023.
- [3] Jeane Camelo, Talea L. Mayo, and Ethan D. Gutmann. Projected climate change impacts on hurricane storm surge inundation in the coastal United States. *Frontiers in Built Environment*, 6, December 2020. ISSN 2297-3362. doi: 10.3389/fbuil.2020.588049. URL <http://dx.doi.org/10.3389/fbuil.2020.588049>.
- [4] Babak Salarieh, Izuchukwu A. Ugwu, and Abdullahi M. Salman. Impact of changes in sea surface temperature due to climate change on hurricane wind and storm surge hazards across US Atlantic and Gulf coast regions. *SN Applied Sciences*, 5(8), July 2023. ISSN 2523-3971. doi: 10.1007/s42452-023-05423-7. URL <http://dx.doi.org/10.1007/s42452-023-05423-7>.
- [5] Natacha B. Bernier, Mark Hemer, Nobuhito Mori, Christian M. Appendini, Oyvind Breivik, Ricardo de Camargo, Mercè Casas-Prat, Trang Minh Duong, Ivan D. Haigh, Tom Howard, Vanessa Hernaman, Oleksandr Huizy, Jennifer L. Irish, Ebru Kirezci, Nadao Kohno, Jun-Whan Lee, Kathleen L. McInnes, Elke M.I. Meyer, Marta Marcos, Reza Marsooli, Ariadna Martin Oliva, Melisa Menendez, Saeed Moghimi, Sanne Muis, Jeff A. Polton, William J. Pringle, Roshanka Ranasinghe, Thomas Saillour, Grant Smith, Michael Getachew Tadesse, Val Swail, Shimura Tomoya, Evangelos Voukouvalas, Thomas Wahl, Pengcheng Wang, Ralf Weisse, Joannes J. Westerink, Ian Young, and Y. Joseph Zhang. Storm surges and extreme sea levels: Review, establishment of model intercomparison and coordination of surge climate projection efforts (SurgeMIP). *Weather and Climate Extremes*, 45:100689, September 2024. ISSN 2212-0947. doi: 10.1016/j.wace.2024.100689. URL <http://dx.doi.org/10.1016/j.wace.2024.100689>.
- [6] R. L. Kolar, W. G. Gray, J. J. Westerink, and R. A. Luettich. Shallow water modeling in spherical coordinates: equation formulation, numerical implementation, and application. *Journal of Hydraulic Research*, 32(1):3–24, January 1994. ISSN 1814-2079. doi: 10.1080/00221689409498786. URL <http://dx.doi.org/10.1080/00221689409498786>.
- [7] Donald T. Resio and Joannes J. Westerink. Modeling the physics of storm surges. *Physics Today*, 61(9):33–38, September 2008. ISSN 1945-0699. doi: 10.1063/1.2982120. URL <http://dx.doi.org/10.1063/1.2982120>.
- [8] J. J. Westerink, R. A. Luettich, A. M. Baptists, N. W. Scheffner, and P. Farrar. Tide and storm surge predictions using finite element model. *Journal of Hydraulic Engineering*, 118(10):1373–1390, October 1992. doi: 10.1061/(asce)0733-9429(1992)118:10(1373).
- [9] J.C. Dietrich, M. Zijlema, J.J. Westerink, L.H. Holthuijsen, C. Dawson, R.A. Luettich, R.E. Jensen, J.M. Smith, G.S. Stelling, and G.W. Stone. Modeling hurricane waves and storm surge using integrally-coupled, scalable computations. *Coastal Engineering*, 58(1):45–65, January 2011. ISSN 0378-3839. doi: 10.1016/j.coastaleng.2010.08.001. URL <http://dx.doi.org/10.1016/j.coastaleng.2010.08.001>.
- [10] Joannes J. Westerink, Richard A. Luettich, Jesse C. Feyen, John H. Atkinson, Clint Dawson, Hugh J. Roberts, Mark D. Powell, Jason P. Dunion, Ethan J. Kubatko, and Hasan Pourtaheri. A basin- to channel-scale unstructured grid hurricane storm surge model applied to southern Louisiana. *Monthly Weather Review*, 136(3):833–864, March 2008. ISSN 0027-0644. doi: 10.1175/2007mwr1946.1. URL <http://dx.doi.org/10.1175/2007MWR1946.1>.
- [11] M. E. Hope, J. J. Westerink, A. B. Kennedy, P. C. Kerr, J. C. Dietrich, C. Dawson, C. J. Bender, J. M. Smith, R. E. Jensen, M. Zijlema, L. H. Holthuijsen, R. A. Luettich, M. D. Powell, V. J. Cardone, A. T. Cox, H. Pourtaheri, H. J. Roberts, J. H. Atkinson, S. Tanaka, H. J. Westerink, and L. G. Westerink. Hindcast and validation of Hurricane Ike (2008) waves, forerunner, and storm surge. *Journal of Geophysical Research: Oceans*, 118(9):4424–4460, September 2013. ISSN 2169-9291. doi: 10.1002/jgrc.20314. URL <http://dx.doi.org/10.1002/jgrc.20314>.

- [12] CERA - Coastal Emergency Risk Assessment. Center for Computation and Technology at Louisiana State University. <https://cera.coastalrisk.live/>, 2024.
- [13] Carola Kaiser, Clinton N. Dawson, Efstratios Nikidis, and Jason G. Fleming. ADCIRC/SWAN hindcasts for historical storms 2003-2022, 2023. URL <https://www.designsafe-ci.org/data/browser/public/designsafe.storage.published/PRJ-3932/#details-5508251847528869395-242ac117-0001-012>.
- [14] CERA - Historical Storm Archive — historicalstorms.coastalrisk.live. <https://historicalstorms.coastalrisk.live/>, 2024. [Accessed 17-08-2024].
- [15] William J. Pringle, Damrongsak Wirasaet, Keith J. Roberts, and Joannes J. Westerink. Global storm tide modeling with ADCIRC v55: unstructured mesh design and performance. *Geoscientific Model Development*, 14(2):1125–1145, February 2021. ISSN 1991-9603. doi: 10.5194/gmd-14-1125-2021. URL <http://dx.doi.org/10.5194/gmd-14-1125-2021>.
- [16] Sina Khani and Clinton N. Dawson. A gradient based subgrid-scale parameterization for ocean mesoscale eddies. *Journal of Advances in Modeling Earth Systems*, 15(2), January 2023. ISSN 1942-2466. doi: 10.1029/2022ms003356. URL <http://dx.doi.org/10.1029/2022MS003356>.
- [17] Coleman P. Blakely, Guoming Ling, William J. Pringle, María Teresa Contreras, Damrongsak Wirasaet, Joannes J. Westerink, Saeed Moghimi, Greg Seroka, Lei Shi, Edward Myers, Margaret Owensby, and Chris Massey. Dissipation and bathymetric sensitivities in an unstructured mesh global tidal model. *Journal of Geophysical Research: Oceans*, 127(5), May 2022. ISSN 2169-9291. doi: 10.1029/2021jc018178. URL <http://dx.doi.org/10.1029/2021JC018178>.
- [18] Mark Loveland, Jessica Meixner, Eirik Valseeth, and Clint Dawson. Efficacy of reduced order source terms for a coupled wave-circulation model in the Gulf of Mexico. *Ocean Modelling*, 190:102387, August 2024. ISSN 1463-5003. doi: 10.1016/j.ocemod.2024.102387. URL <http://dx.doi.org/10.1016/j.ocemod.2024.102387>.
- [19] Victor M. Gonzalez, Norberto C. Nadal-Caraballo, Jeffrey A. Melby, and Mary A. Cialone. Quantification of uncertainty in probabilistic storm surge models: Literature review. Technical report, U.S. Army Corps of Engineers, Engineer Research and Development Center, 2019. URL https://chs.erd.c.dren.mil/Library/References/CHS_PCHA_Publications/Reports/SR-19-1_Gonzalez_et_al_2019_UncertaintyInSurgeModels.pdf.
- [20] Celso M. Ferreira, Jennifer L. Irish, and Francisco Olivera. Uncertainty in hurricane surge simulation due to land cover specification. *Journal of Geophysical Research: Oceans*, 119(3):1812–1827, March 2014. ISSN 2169-9275. doi: 10.1002/2013jc009604. URL <http://dx.doi.org/10.1002/2013JC009604>.
- [21] Marissa J. Torres, M. Reza Hashemi, Scott Hayward, Malcolm Spaulding, Isaac Ginis, and Stephan T. Grilli. Role of hurricane wind models in accurate simulation of storm surge and waves. *Journal of Waterway, Port, Coastal, and Ocean Engineering*, 145(1), January 2019. ISSN 1943-5460. doi: 10.1061/(asce)ww.1943-5460.0000496. URL [http://dx.doi.org/10.1061/\(ASCE\)WW.1943-5460.0000496](http://dx.doi.org/10.1061/(ASCE)WW.1943-5460.0000496).
- [22] Timu W. Gallien, Nikos Kalligeris, Marie-Pierre C. Delisle, Bo-Xiang Tang, Joseph T. D. Lucey, and Maria A. Winters. Coastal flood modeling challenges in defended urban backshores. *Geosciences*, 8(12):450, December 2018. ISSN 2076-3263. doi: 10.3390/geosciences8120450. URL <http://dx.doi.org/10.3390/geosciences8120450>.
- [23] David F. Muñoz, Peyman Abbaszadeh, Hamed Moftakhari, and Hamid Moradkhani. Accounting for uncertainties in compound flood hazard assessment: The value of data assimilation. *Coastal Engineering*, 171:104057, January 2022. ISSN 0378-3839. doi: 10.1016/j.coastaleng.2021.104057. URL <http://dx.doi.org/10.1016/j.coastaleng.2021.104057>.
- [24] Taylor G. Asher, Richard A. Luettich Jr., Jason G. Fleming, and Brian O. Blanton. Low frequency water level correction in storm surge models using data assimilation. *Ocean Modelling*, 144:101483, December 2019. ISSN 1463-5003. doi: 10.1016/j.ocemod.2019.101483. URL <http://dx.doi.org/10.1016/j.ocemod.2019.101483>.
- [25] Donald T. Resio, Jennifer L. Irish, Joannes J. Westerink, and Nancy J. Powell. The effect of uncertainty on estimates of hurricane surge hazards. *Natural Hazards*, 66(3):1443–1459, October 2012. ISSN 1573-0840. doi: 10.1007/s11069-012-0315-1. URL <http://dx.doi.org/10.1007/s11069-012-0315-1>.
- [26] T. Butler, M. U. Altaf, C. Dawson, I. Hoteit, X. Luo, and T. Mayo. Data assimilation within the Advanced Circulation (ADCIRC) modeling framework for hurricane storm surge forecasting. *Monthly Weather Review*, 140(7):2215–2231, July 2012. ISSN 1520-0493. doi: 10.1175/mwr-d-11-00118.1. URL <http://dx.doi.org/10.1175/MWR-D-11-00118.1>.
- [27] Thomas Höllt, M. Umer Altaf, Kyle T. Mandli, Markus Hadwiger, Clint N. Dawson, and Ibrahim Hoteit. Visualizing uncertainties in a storm surge ensemble data assimilation and forecasting system. *Natural Hazards*, 77(1):317–336, January 2015. ISSN 1573-0840. doi: 10.1007/s11069-015-1596-y. URL <http://dx.doi.org/10.1007/s11069-015-1596-y>.
- [28] Delei Li, Jianlong Feng, Zhenhua Xu, Baoshu Yin, Hongyuan Shi, and Jifeng Qi. Statistical bias correction for simulated wind speeds over CORDEX-East Asia. *Earth and Space Science*, 6(2):200–211, February 2019. ISSN 2333-5084. doi: 10.1029/2018ea000493. URL <http://dx.doi.org/10.1029/2018EA000493>.
- [29] Fang Wang and Di Tian. On deep learning-based bias correction and downscaling of multiple climate models simulations. *Climate Dynamics*, 59(11–12):3451–3468, April 2022. ISSN 1432-0894. doi: 10.1007/s00382-022-06277-2. URL <http://dx.doi.org/10.1007/s00382-022-06277-2>.
- [30] Stefanos Giaremsis, Noujoud Nader, Clint Dawson, Carola Kaiser, Efstratios Nikidis, and Hartmut Kaiser. Storm surge modeling in the AI era: Using LSTM-based machine learning for enhancing forecasting accuracy. *Coastal Engineering*, 191:104532, August 2024. ISSN 0378-3839. doi: 10.1016/j.coastaleng.2024.104532. URL <http://dx.doi.org/10.1016/j.coastaleng.2024.104532>.
- [31] Danyi Sun, Wenyu Huang, Yong Luo, Jingjia Luo, Jonathon S. Wright, Haohuan Fu, and Bin Wang. A deep learning-based bias correction method for predicting ocean surface waves in the northwest pacific ocean. *Geophysical Research Letters*, 49(23), December 2022. ISSN 1944-8007. doi: 10.1029/2022gl100916. URL <http://dx.doi.org/10.1029/2022GL100916>.
- [32] Ricardo Martins Campos, Vladimir Krasnopolsky, Jose-Henrique Alves, and Stephen G. Penny. Improving NCEP’s global-scale wave ensemble averages using neural networks. *Ocean Modelling*, 149:101617, May 2020. ISSN 1463-5003. doi: 10.1016/j.ocemod.2020.101617. URL <http://dx.doi.org/10.1016/j.ocemod.2020.101617>.

- [33] Ashley Ellenson, Yuanli Pei, Gregory Wilson, H. Tuba Özkan Haller, and Xiaoli Fern. An application of a machine learning algorithm to determine and describe error patterns within wave model output. *Coastal Engineering*, 157:103595, April 2020. ISSN 0378-3839. doi: 10.1016/j.coastaleng.2019.103595. URL <http://dx.doi.org/10.1016/j.coastaleng.2019.103595>.
- [34] Ian Goodfellow, Jean Pouget-Abadie, Mehdi Mirza, Bing Xu, David Warde-Farley, Sherjil Ozair, Aaron Courville, and Yoshua Bengio. Generative adversarial networks. *Communications of the ACM*, 63(11):139–144, 2020.
- [35] Ian Goodfellow, Jean Pouget-Abadie, Mehdi Mirza, Bing Xu, David Warde-Farley, Sherjil Ozair, Aaron Courville, and Yoshua Bengio. Generative adversarial nets. In Z. Ghahramani, M. Welling, C. Cortes, N. Lawrence, and K.Q. Weinberger, editors, *Advances in Neural Information Processing Systems*, volume 27. Curran Associates, Inc., 2014. URL https://proceedings.neurips.cc/paper_files/paper/2014/file/5ca3e9b122f61f8f06494c97b1afccf3-Paper.pdf.
- [36] Xiaohui Li, Xinhai Han, Jingsong Yang, Jiuke Wang, and Guoqi Han. Transfer learning-based generative adversarial network model for tropical cyclone wind speed reconstruction from SAR images. *IEEE Transactions on Geoscience and Remote Sensing*, 62:1–16, 2024. ISSN 1558-0644. doi: 10.1109/tgrs.2024.3390392. URL <http://dx.doi.org/10.1109/TGRS.2024.3390392>.
- [37] Bastien François, Soulivanh Thao, and Mathieu Vrac. Adjusting spatial dependence of climate model outputs with cycle-consistent adversarial networks. *Climate Dynamics*, 57(11–12):3323–3353, July 2021. ISSN 1432-0894. doi: 10.1007/s00382-021-05869-8. URL <http://dx.doi.org/10.1007/s00382-021-05869-8>.
- [38] R. El Osta, A. Sajeewan, and N. Nader. Climate change analysis using earth’s surface temperature: Hierarchical time series. *International Journal of Data Science and Advanced Analytics*, 6(6), 2024. doi: <https://doi.org/10.69511/ijdsaa.v6i6.234>.
- [39] Baoxiang Pan, Gemma J. Anderson, André Goncalves, Donald D. Lucas, Céline J. W. Bonfils, Jiwoo Lee, Yang Tian, and Hsi-Yen Ma. Learning to correct climate projection biases. *Journal of Advances in Modeling Earth Systems*, 13(10), October 2021. ISSN 1942-2466. doi: 10.1029/2021ms002509. URL <http://dx.doi.org/10.1029/2021MS002509>.
- [40] Jinsung Yoon, Daniel Jarrett, and Mihaela Van der Schaar. Time-series generative adversarial networks. *Advances in neural information processing systems*, 32, 2019.
- [41] NOAA. Water levels - station selection, 2023. URL <https://tidesandcurrents.noaa.gov/stations.html>.
- [42] USGS. Usgs current water data for the nation, 2023. URL <https://waterdata.usgs.gov/nwis/rt>.
- [43] US Army Corps of Engineers. Rivergages.com: Providing River Gage Data for Rivers, Streams and Tributaries — rivergages.mvr.usace.army.mil. <https://rivergages.mvr.usace.army.mil/WaterControl/new/layout.cfm>. [Accessed 19-06-2025].
- [44] NOAA Tides & Currents — tidesandcurrents.noaa.gov. <https://tidesandcurrents.noaa.gov/tcoon.html>. [Accessed 19-06-2025].
- [45] Puerto Rico Seismic Network — prsn.uprm.edu. <http://www.prsn.uprm.edu/English/tidesgauges/index.php>. [Accessed 19-06-2025].
- [46] Saffir-Simpson Hurricane Scale — weather.gov. <https://www.weather.gov/mfl/saffirsimpson>. [Accessed 31-05-2025].
- [47] Kristina P Sinaga and Miin-Shen Yang. Unsupervised k-means clustering algorithm. *IEEE access*, 8:80716–80727, 2020.
- [48] Fabian Pedregosa, Gaël Varoquaux, Alexandre Gramfort, Vincent Michel, Bertrand Thirion, Olivier Grisel, Mathieu Blondel, Peter Prettenhofer, Ron Weiss, Vincent Dubourg, et al. Scikit-learn: Machine learning in python. *the Journal of machine Learning research*, 12:2825–2830, 2011.
- [49] Z.B. Akhtar. Unveiling the evolution of generative ai (gai): a comprehensive and investigative analysis toward llm models (2021–2024) and beyond. *Journal of Electrical Systems and Inf Technol*, 11(22), 2024. doi: <https://doi.org/10.1186/s43067-024-00145-1>.
- [50] S.S. Sengar, A.B. Hasan, and S. et al. Kumar. Generative artificial intelligence: a systematic review and applications. *Multimed Tools Appl* (2024), 2024. doi: <https://doi.org/10.1007/s11042-024-20016-1>.
- [51] Diederik P Kingma and Jimmy Ba. Adam: A method for stochastic optimization. *arXiv preprint arXiv:1412.6980*, 2014.

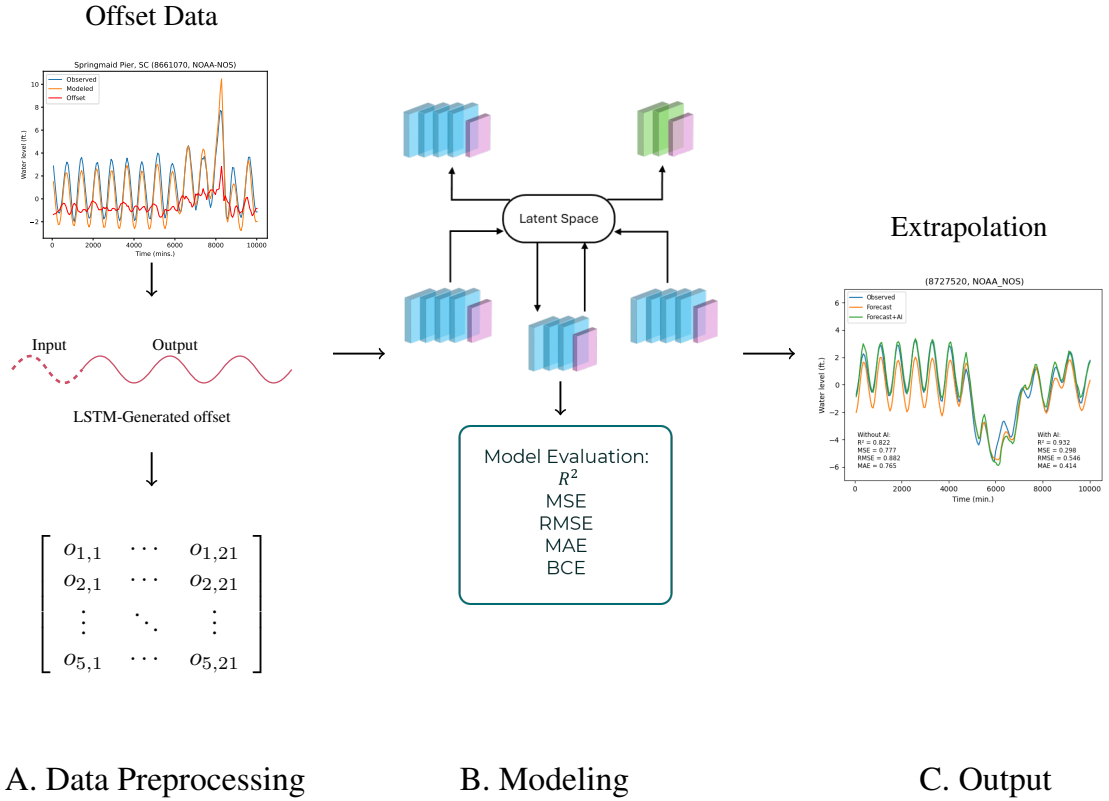


Figure 1: Overview of the methodology framework: (A) Data Pre-processing phase includes offset extraction using Eq. 2.1, data cleaning, and normalization. (B) Modeling phase involves the structure of the TimeGAN components and model evaluation using regression metrics. (C) Output phase includes the final application of the pre-trained model for bias extrapolation. The generated offsets are then used to correct the forecasted data using Eq. 2.2.

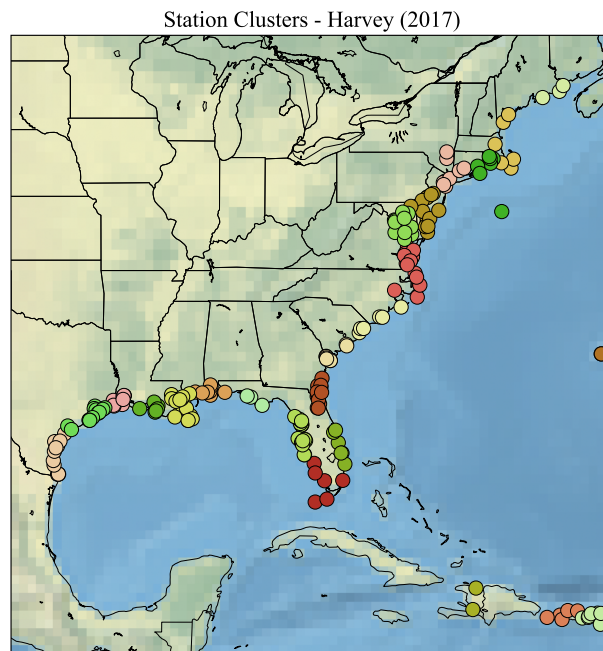


Figure 2: Station clustering for Hurricane Harvey (2017). This map illustrates the clustering of stations based on their coordinates. A total of 24 clusters were identified, with each color representing a different cluster.

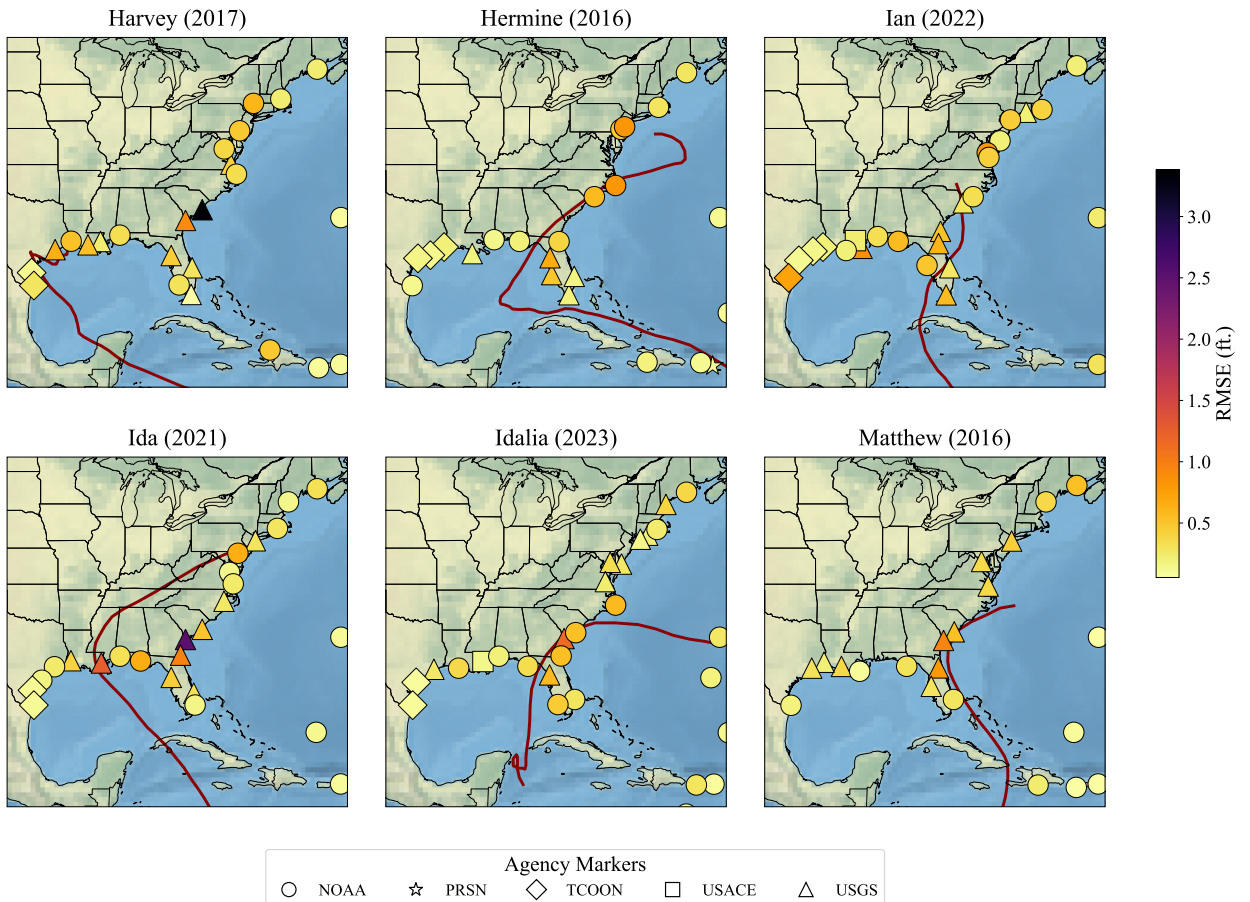


Figure 3: RMSE values for the testing stations across different hurricanes. The map for each hurricane shows the locations of the testing stations along with their corresponding RMSE values (in feet), indicated by the color gradient. The considered hurricanes are Harvey (2017), Hermine (2016), Ian (2022), Ida (2021), Idalia (2023), and Matthew (2016) and the considered agencies are NOAA, USACE, USGS, TCOON, and PRSN. The hurricane paths are outlined in red.

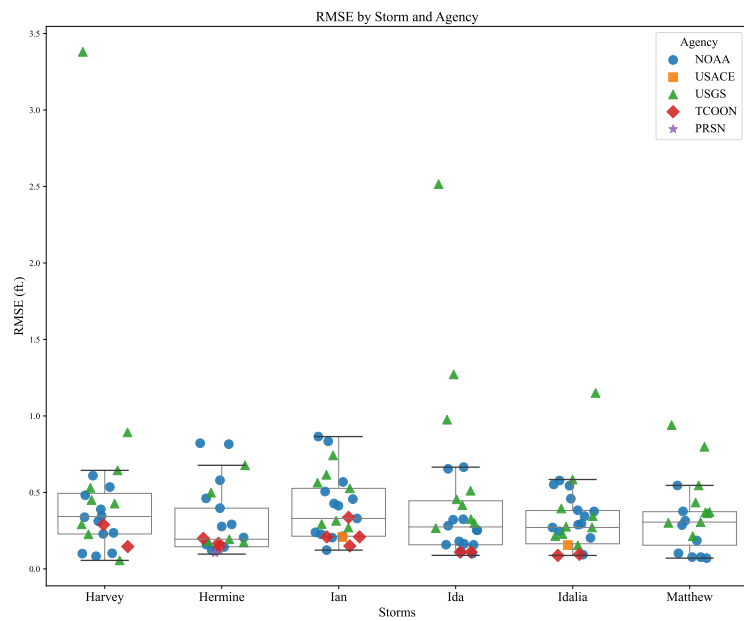


Figure 4: RMSE distribution of the extrapolated offsets with the HURRI-GAN model in the testing stations by hurricane and agency. The considered hurricanes are Harvey (2017), Hermine (2016), Ian (2022), Ida (2021), Idalia (2023), and Matthew (2016) and the considered agencies are NOAA, USACE, USGS, TCOON, and PRSN.

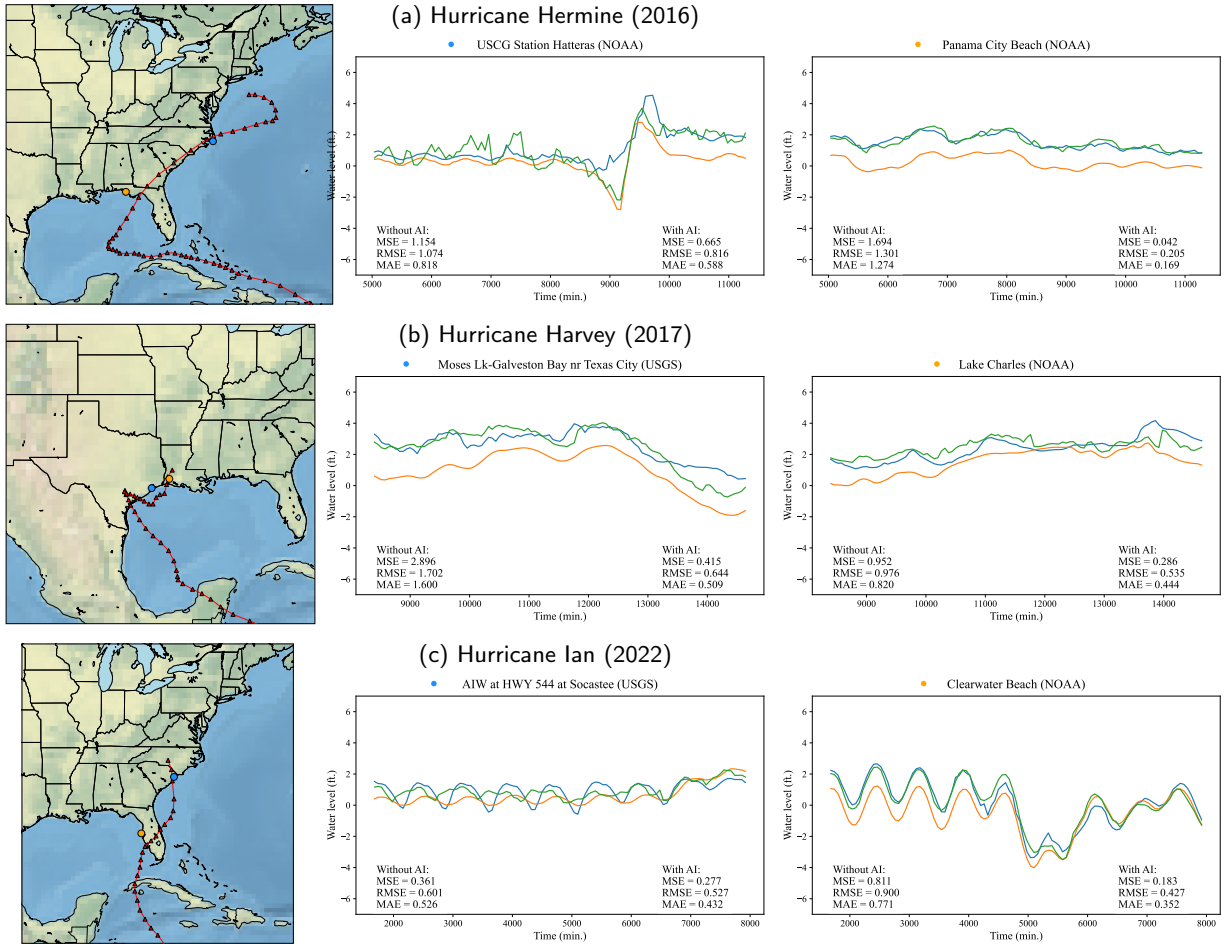


Figure 5: Comparison of observed (blue), modeled (orange) and HURRI-GAN-corrected modeled (green) for: (a) Hermine (2016, category H1), (b) Harvey (2017, category H4), and (c) Ian (2022, category H5). The left side displays the location of two testing gauge stations (marked by colored disks) and the hurricane path (in red); while the right side shows the evaluation of the regression performance for these gauge stations. Evaluation statistics in each plot represent the performance of regression between modeled and observed water levels (without AI) and HURRI-GAN bias corrected and observed water levels (with AI).

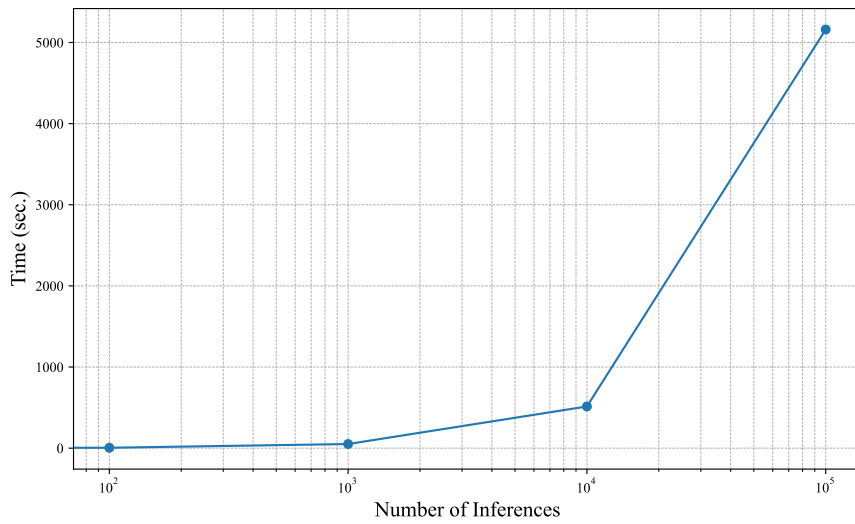


Figure 6: Computational time (in seconds) required for the HURRI-GAN model to sequentially extrapolate bias corrections (i.e., inference time), as a function of the total amount of corrections.